Multiscale mechanical model for cell division orientation in developing biological systems

B. Leggio*,[1,2] J. Laussu,[2] E. Faure,[1,2,3] P. Lemaire,[2] and C. Godin[1]

[1] *Laboratoire Reproduction et Développement des Plantes (LRDP), Univ Lyon, ENS de Lyon, UCB Lyon 1, CNRS, INRA, Inria, Lyon 69342, France*

[2] *Centre de Recherche de Biologie cellulaire de Montpellier (CRBM), Univ Montpellier, CNRS, Montpellier 34293, France*

[3] *Laboratoire d'Informatique de Robotique et de Microélectronique de Montpellier (LIRMM), Univ Montpellier, CNRS, Montpellier 34095, France*

Developing biological structures are highly complex systems, within which a robust and efficient information transfer must happen to coordinate several dynamical processes. Through a reformulation of cytokinesis in terms of its energetic cost, we propose that oriented cell divisions are one mechanism by which cells can read and react to mechanical forces propagating in a tissue even in the absence of cellular strain. This view can at once account for the standard geometrical rules for cell division, as much as the known systematic deviations from them. Our results suggest the existence of a shape-dynamics to cell-division feedback loop, consisting in the competition between local and long-range mechanical signals. The consequences of this competition are explored in simulated tissues and confirmed *in vivo* during the epidermal morphogenesis of ascidian embryos.

I. INTRODUCTION

In a developing biological system several dynamical processes take place at specific positions in order to produce and change the system's shape. These local processes leading to shape changes need either to be tightly coordinated or dynamically adjusted to ensure global coherence [1–3]. There must hence exist mechanisms through which shape dynamics information is transferred and read. The nature of such information, and how it propagates is an important, yet open question.

Thanks to the burst of new technologies and the consequent availability of quantitative morphodynamic data [4–7], the dynamics of shapes and its robustness against environmental and intrinsic noise is being investigated under a new paradigm, in which the shape itself drives its own change by feeding back on its own functioning. Several works have shown different aspects of this general idea [8–16]. One important process known to be driven by cell shape is cell division. In both animal and plant tissues the orientation of a cell's division plane often aligns orthogonal to the long geometrical axis of the dividing cell (Hertwig's rule, or HR, in animals [17–19], Errera's rule in plants [20, 21]). The emergence of these rules in animal cells has been linked to the action of mechanical forces [19, 22, 23]. In all these cases the predicted rule is in very good agreement with the direction of the cell's long-axis. Despite the generality of such phenomenological laws, systematic and reproducible deviations from them are not rare [24–27]. Such deviations are often found to correlate with states of anisotropic tension in the surrounding tissue. A theoretical picture of such systematic deviations in connection to mechanical stress has only recently started being developed [25], but its general understanding is still largely missing.

Cell division is, in several contexts, also a process which actively changes the shape of cells [12, 28, 29], above all in animal tissues. Cells increase their volume, expand their apical surface, or generally alter their form before, during and after cytokinesis [29–31]. Dividing animal cells push against their neighbours to create space to accommodate shape changes and volume increase during and after mitosis [12]. If a cell's environment is too stiff for the cell to deform it, the so-called spindle assembly checkpoint prevents progression to anaphase and stalls the division process. Division is thus a process in which the cell's surroundings feeds back information, used by the cell to regulate its mitosis.

In this work, we develop a theoretical model of a shape-division feedback loop, which can at once account for HR and systematic devia-

*Corresponding author: bruno.leggio@inria.fr

tions from it. We argue that, not differently from other physical phenomena, cell division minimizes (mechanical) energy dissipation by putting together contributions from both short- and long-range shape information. Such information is mechanically supplied to (and integrated by) a dividing cell and used as a cue to orient its division plane, which contributes to ensuring a global long-range coherence to evolving biological forms.

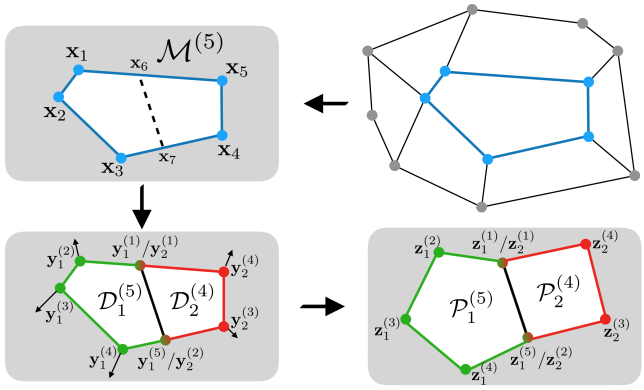

FIG. 1: 2D representation of cell division in a viscous environment. A cell with 5 neighbours and a given rest shape ($\mathcal{M}^{(5)}$) divides, creating two daughter cells with, respectively, 5 and 4 neighbours and shapes $\mathcal{D}_1^{(5)}$ and $\mathcal{D}_2^{(4)}$. These two cells deform their surrounding environment to achieve regular vertices distribution and increase their total area, tending to target shapes $\mathcal{P}_1^{(5)}$ and $\mathcal{P}_2^{(4)}$. $\mathcal{D}_1^{(5)}$, $\mathcal{D}_2^{(4)}$, $\mathcal{P}_1^{(5)}$ and $\mathcal{P}_2^{(4)}$ depend on the orientation $\mathbf{n}$ of division plane. Each vertex follows a trajectory $\tau^{(i)}(\hat{\mathbf{n}})$ from its initial position $\mathbf{y}^{(i)}$ to its target position $\mathbf{z}^{(i)}$.

II. CELL DIVISION IN CROWDED ENVIRONMENTS

A. Shape dynamics

In a multicellular system, global equilibrium comes from the competition between interacting bodies trying to minimize their configurational energy. Under normal conditions, this energy for an isolated cell is minimized for spherical shape due to the cell's cortical tension [32]. The global shape of a 2D tissue is often abstracted as the positions $\mathbf{R}_i$ of its cellular junctions, represented as vertices of a collection of polygons in the widely-employed representation known as vertex-based cellular model [33]. The dynamics of these vertices has largely been studied and is well captured by the single-cell Hamiltonian [33]

$$\mathcal{H}_c^{\mathrm{V}} = \lambda_c P_c + \kappa_c \big(A_c - A_c^{(0)}\big)^2, \tag{1}$$

in terms of cortical tension λ_c along the cell perimeter P_c and surface elasticity κ_c of the cell area A_c around an equilibrium surface $A_c^{(0)}$. The latter accounts at once for volume compressibility and for the actomyosin-mediated elastic properties of a cell's surface. Locally, the equilibrium shape $\mathcal{M} = \{\mathbf{R}_i\}$ can be altered either by regulation of λ_c, κ_c and $A_c^{(0)}$ or by individual-cell active events such as cell migration, division and death.

B. Cell division in multicellular systems: an energetic viewpoint

In tightly-packed tissues, shape changes during mitosis have an energetic cost [12] which is a consequence of the cell-cell competition for space. In [24], a model for the influence of direct neighbours on a cell's division orientation was given in terms of cell topology. However, only relatively small deviations from geometric rules were predicted, and no connection to mechanical stress patterns was studied. The results of [12] suggest a strong connection between cell division regulation and the amount of a cell's internal energy flowing to its environment by mechanical forces. No physical model has been developed yet to study this phenomenon: filling this gap is the main contribution of our work.

Biological tissues are usually modelled as non-equilibrium viscoelastic mechanical systems [9], with properties changing with time and observation scale. In many circumstances one can, however, model the resistance offered by biological matter to displacement as a fluid with viscosity η. Due to the viscosity of the medium, energy is consumed in the work of friction forces W_η in the surrounding tissue as

$$\frac{W_\eta}{\eta} = \sum_{i=1}^{\kappa_1} \int_{\tau_1^{(i)}(\hat{\mathbf{n}})} \mathbf{v}_1^{(i)} \cdot \mathrm{d}\mathbf{p}_1^{(i)} + \sum_{j=1}^{\kappa_2} \int_{\tau_2^{(j)}(\hat{\mathbf{n}})} \mathbf{v}_2^{(j)} \cdot \mathrm{d}\mathbf{p}_2^{(j)}, \tag{2}$$

where $\tau^{(i)}_{1(2)}(\hat{\mathbf{n}})$ is the trajectory followed by the i-th vertex of daughter cell 1 (2), which depends on the division orientation $\hat{\mathbf{n}}$, $\mathbf{p}^{(i)}_{1(2)}(t)$ its instantaneous position along the trajectory, $\mathbf{v}^{(i)}_{1(2)}(t)$ its finite velocity, $\sum^{\kappa_1}$ ($\sum^{\kappa_2}$) runs over all κ_1 (κ_2) vertices of daughter cell 1 (2) (common vertices contribute with weight 1/2 in both sums). The work (2) depends on the amount of deformation required to accommodate the daughters' final shape, as schematically shown in Fig. 1. A natural consequence of this is that different division orientations correspond to different amounts of energy consumed by the dividing cell $\Delta U^c(\hat{\mathbf{n}}) = -W_\eta$. Such a formulation of the energetic cost of cell division (and its generalization, see Eq. (4) in the following) is the first contribution of this work.

Cells or tissues also actively change their shape, as a result of intra-cellular processes and/or the effect of external interactions. A local change in shape implies the build-up of mechanical forces within the tissue, which propagate at more or less long distance depending on the properties of the cellular medium. Be $\{\sigma\}$ the set of cells or multicellular structures whose shape is being actively changed. Any point $\mathbf{r}$ in the tissue will feel a force exerted by each of these structures, along a direction $\hat{\mathbf{w}}_\sigma(\mathbf{r})$ and of intensity ψ_σ. The total force at a position $\mathbf{r}$ within the tissue is

$$\mathbf{F}(\mathbf{r}) = \sum_\sigma \psi_\sigma \hat{\mathbf{w}}_\sigma(\mathbf{r}) = \sum_\sigma F_\sigma \mathbf{f}_\sigma(\mathbf{r}), \qquad (3)$$

having written $\psi_\sigma = F_\sigma f\big(d(\mathbf{r}, \mathcal{O}_\sigma)\big)$, where F_σ is the force intensity at the position of the process σ, $f(x)$ is a monotonically decreasing function and $d(\mathbf{r}, \mathcal{O}_\sigma)$ is the euclidean distance between $\mathbf{r}$ and the structure σ. Finally, $\mathbf{f}_\sigma(\mathbf{r}) = \hat{\mathbf{w}}_\sigma(\mathbf{r}) f\big(d(\mathbf{r}, \mathcal{O}_\sigma)\big)$. These forces exert mechanical work on vertices of a dividing cell. The total change in a cell's internal energy during division is thus due to the energy spent against friction forces plus the work performed by the external forces (3) and reads

$$\frac{\Delta U^c(\hat{\mathbf{n}})}{\eta} = \sum_{i=1}^{\kappa_1} \int_{\tau_1^{(i)}(\hat{\mathbf{n}})} \left(\sum_\sigma \phi_\sigma \mathbf{f}_\sigma(\mathbf{p}_1^{(i)}) - \mathbf{v}_1^{(i)} \right) \cdot \mathrm{d}\mathbf{p}_1^{(i)} + \sum_{j=1}^{\kappa_2} \int_{\tau_2^{(j)}(\hat{\mathbf{n}})} \left(\sum_\sigma \phi_\sigma \mathbf{f}_\sigma(\mathbf{p}_2^{(j)}) - \mathbf{v}_2^{(j)} \right) \cdot \mathrm{d}\mathbf{p}_2^{(j)}. \quad (4)$$

ΔU^c stems from the multiscale competition between the local, passive contribution of Eq. (2) and the active, long-range effect of Eq. (3), and is a function of the cell's division orientation through the trajectories $\tau^{(i)}(\hat{\mathbf{n}})$. This competition is captured by the ratio $\phi_\sigma = \frac{F_\sigma}{\eta}$. This is the cornerstone of our work and provides an energetic standpoint to understand energy fluxes between a dividing cell and its local and far-away environments. It provides a quantitative ground to study oriented cell division by allowing the identification of the most energetically-favourable set of trajectories for cell division, given by the direction $\hat{\mathbf{n}}_0$ maximising Eq. (4). It is worth stressing here that effect of mechanical forces in Eq. (4) is fully independent of the possible strain they induce on the cell. This is indeed what was observed in several *in vivo* situations [26, 27]: mechanical stress in a tissue correlates with division orientations even in the absence of strain, leading to systematic violations of geometric rules for cell division.

III. EMERGING BEHAVIOURS

A. Isolated tissues

Equation (4) has several interesting consequences. For isolated tissues in the absence of mechanical cues ($\phi_\sigma = 0$), geometrical rules for cell divisions are expected to be followed. The local part of Eq. (4), i.e., (2), is able to account for and physically explain this fact, as shown in Fig. 2 for 10^4 cells, whose shape and vertices dis-

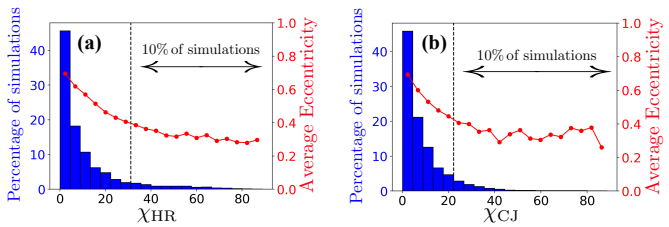

FIG. 2: Distribution of deviation angles $\chi_{\rm HR} = \arccos|\hat{\mathbf{n}}_0 \cdot \hat{\mathbf{n}}_{\rm HR}|$ (a) and $\chi_{\rm CJ} = \arccos|\hat{\mathbf{n}}_0 \cdot \hat{\mathbf{n}}_{\rm CJ}|$ (b) for 10^4 randomly simulated cells. Here $\hat{\mathbf{n}}_0$ minimizes Eq. (2); $\hat{\mathbf{n}}_{\rm HR}$ is the cell's main elongation axis and $\hat{\mathbf{n}}_{\rm CJ}$ the main direction of cellular junctions. Red points (right vertical scale) give the average eccentricity of the ellipses approximating each cell in each histogram bar. 90% of cells have $\chi_{\rm CJ} < 22°$ and $\chi_{\rm HR} < 30°$, in agreement with what is found *in vivo* [19].

tribution was randomly simulated as explained in Appendix A. For each of them, Eq. (2) was numerically minimized assuming linear trajectories $\tau_k^{(i)}$. As shown in Fig. 2, the energetically optimal direction $\hat{\mathbf{n}}_0$ minimizing Eq. (2) correlates with both the main elongation axis $\hat{\mathbf{n}}_{\rm HR}$ and the principal direction cell junctions (in our model, its vertices) $\hat{\mathbf{n}}_{\rm CJ}$. Interestingly, the agreement of Eq. (2) to $\hat{\mathbf{n}}_{\rm CJ}$ is higher than to $\hat{\mathbf{n}}_{\rm HR}$, motivating cell junctions as the main geometrical cue for division orientation in 2D structures, as shown in [19].

This is our first main result, which shows how cells following geometric rules have an energetic advantage. This property is however not able to explain the full phenomenology of oriented cell divisions and HR violations observed in living systems.

B. Multicellular structures under mechanical stress: a paradigm to understand embryonic morphogenesis

To study the consequences of the competition between local viscosity and long-range propagation of mechanical forces, we analysed the situation depicted in Fig. 3(a) in which one shrinking structure exerts a force $\phi_0\mathbf{f}_0$ on a simulated system initially composed of n cells, with characteristic linear dimension L_0, undergoing three rounds of cell divisions. Such is the case in a number of developing animal embryos, during the shape changing process known as gastrulation [35]. In particular, the situation in Fig. 3(a) illustrates the process of epidermal morphogenesis during gastrulation in embryos of the ascidian *P. mammillata*, a model organism to study animal morphogenesis [36]. Around 4 hours after fertilization, these embryos undergo radical shape change processes, collectively known as gastrulation, which begin with the invagination of a group of cells [37], whose active shape changes drive the whole process as schematically depicted in Fig. 3(b) (see also Fig. B.1). Part of the epidermis of these embryos is at one- to few-cell distance from the gastrulating core and is hence subject to the mechanical stress it produces. Interestingly, during these processes no cell migration nor cell death is known to happen. Thanks to the transparency of these embryos and to state-of-the-art 3D reconstruction of live embryonic development, high-quality 3D dynamic data on their development is now available [34]. Remarkably, ascidian embryos develop with a fixed lineage, which allows to identify homologous cells across several different embryos. We have hence calculated, as detailed in Appendix B, the deviation $\Delta_{\rm HR}$ from HR for each epidermal cell across three rounds of cell divisions in two different embryos. The average value across all divisions and all embryos is shown in Fig. 3(c), projected on the 24 cells at the 64-cell stage which will give rise to epidermis. A pattern of deviations emerges, for cells mostly localised around the tissue border. This makes the epidermal morphogenesis of *P. mammillata* an ideal system to test our theory.

Assuming a constant vertex displacement speed ν one can introduce the dimensionless order parameter $\rho = \frac{\phi_0}{\nu}$, measuring the relative intensity of external to viscous forces. Stress decay is assumed here a time-dependent exponential of typical length-scale $L_\delta(t) = \delta(t)L_d$ ($\delta(t) = 1$ for the first two divisions and $\delta(t) = 2$ for the last), in order to account for the increased density of cell junctions which help generating tissue-scale stress profiles [38]. The fractional stress decay length is $\zeta = L_d/L_0$. Between divisions, the system evolves towards its equilibrium accord-

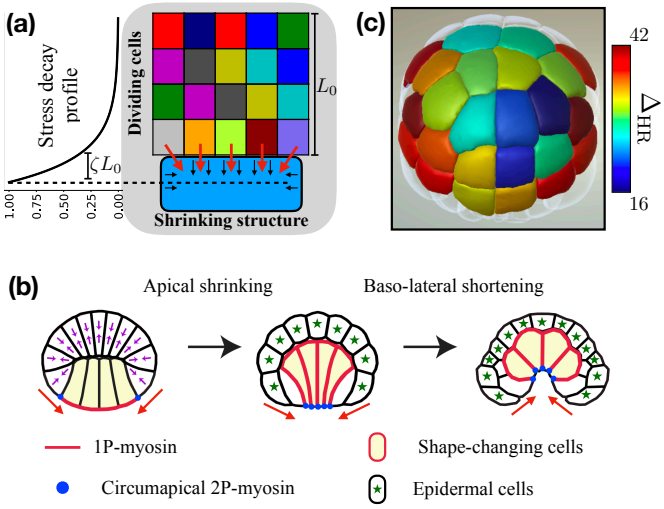

FIG. 3: System of 20 cells, of characteristic linear dimension L_0, in contact with a shrinking structure (panel **(a)**), with exponentially-decaying stress profile of length scale ζL_0. This serves as a model to study the morphogenesis of the epidermis of embryos of *P. mammillata* during gastrulation (panel **(b)**, adapted from [37]). Thanks to the invariant lineage of ascidian embryos, homologous cells can be identified in different embryos. Panel **(c)** shows the average angular deviation $\Delta_{\rm HR}$ (in degree) from HR for three rounds of divisions in ascidian epidermis. The average for each cell is taken over all divisions and across two embryonic datasets, taken from [34] and visualised through the morphological browser MorphoNet [7].

ing to the Hamiltonian $H = \sum \mathcal{H}_c^{\rm V}$ with parameters initially fixed at $\lambda_c/(\kappa_c L_0^3) = 7 \times 10^{-6}$, to account for cell volume incompressibility. Note that no effect of external stress on individual cell shape during interphase has been taken into account. This simplification allows us to decouple the purely-stress-induced effect on tissue shape from the strain-induced effect, and is motivated by the high value of $\kappa_c L_0^3$ compared to the simulated values of force intensities. The agreement between Eq. (4) and the geometrical rules for cell division is captured by the parameter $\alpha = 1 - \langle \chi_{\rm CJ} \rangle / 90$, with $\langle \chi_{\rm CJ} \rangle = \langle \arccos |\hat{\mathbf{n}}_0 \cdot \hat{\mathbf{n}}_{\rm CJ}| \rangle$, the average being taken over every cells at each round of division. α is 1 for perfectly aligned and 0 for fully orthogonal predictions.

The left plot of figure 4(a) shows α as a function of ρ and ζ. Two phases appear in the response of the system: as expected at low ρ (dominant viscosity), Eq. (4) correlates very well with individual-cell geometry; increasing ρ, however, the system undergoes a behavioral phase transition of the continuous type at a critical value ρ_c of the order parameter. At high ρ a new phase emerges in which the agreement between Eq. (4) and cell geometry is rapidly lost (α sharply decreases). To understand the cause of this phase transition we looked at the correlations between cells within the simulated tissue. It is known that the agreement to geometrical rules give rise to alternating orthogonal directions for division orientations within one clone [22]. For a set of initial cells $S_c^{(0)}$ consider the parameter

$$\gamma = \left\langle |\mathbf{n}_t^{(c)} \cdot \mathbf{n}_{t+1}^{(c)}| \right\rangle_{t, c \in S_c^{(0)}}, \tag{5}$$

measuring the correlation between the predicted orientations $\mathbf{n}$ of any two consecutive divisions at t and $t+1$ within the same clone (the set of progeny of a single initial cell) of any cell $c \in S_c^{(0)}$. The average is taken over all cells and all pairs of consecutive division rounds. Figure 4(a) (right) and 4(b) show that the transition to the new phase in the tissue is correlated to by the appearance of time-correlations within each clone. These time-correlations are in turn induced by the stress dynamics within the tissue. To test the influence of mechanical relaxation parameters of Eq. (1), simulations at fixed $\zeta = 1/6$ were run with random values for $\lambda_c/(\kappa_c L_0^3)$, drawn out of a Gaussian distribution centered around $r_0 = 7 \times 10^{-6}$ and of width 10^{-6}. Figure 4(b) shows, for each simulated value of ρ, the average and the standard deviation (in black vertical bars) for 20 random values of $\lambda_c/(\kappa_c L_0^3)$.

The onset of time correlations γ past the critical value ρ_c suggests that the shape of clones may be strongly altered in the presence of external forces, even without individual-cell strain, simply due to time correlations between division orientations and shape changes during cytokinesis. This is indeed the case, as shown in Fig. 4(c): past the critical value ρ_c, clones start showing a more elongated form, tending to a linear shape at high ρ values. This also affects the global tissue shape, which tends to follow the change in shape of the external shrinking structure. The two phases can coexist in the same tissue, as shown in the rightmost example of 4(c), in which the cells facing away from the external force are

in the viscosity-dominated phase and follow geometrical rules ($\alpha = 0.9, \gamma = 0.2$), while the ones directly facing the force are in a stress-dominated phase with high temporal correlations and high deviations from geometry ($\alpha = 0.4, \gamma = 0.8$).

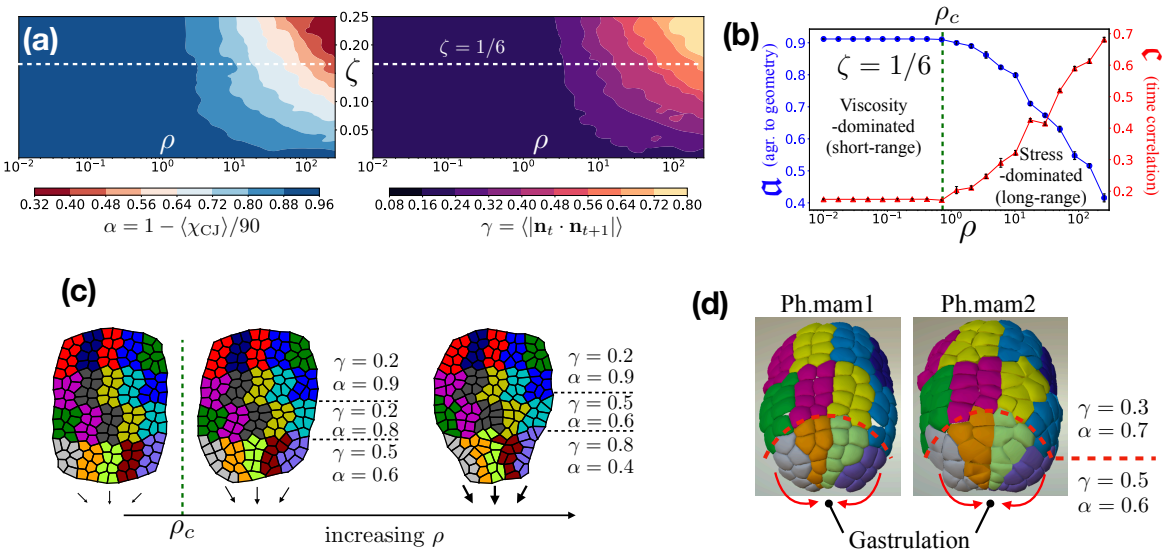

FIG. 4: Panels **(a)** and **(b)** show the predictions of Eq. (4) for the simulated system of Fig. 3(a). A marked transition is found between two phases, (panel **(a)**), for both the agreement of Eq. (4) to geometrical rules α and the average time-correlation of division orientations in clones γ, as a function of the order parameters ρ and ζ. The first phase, (viscosity-dominated, low ρ) shows a high agreement α to the geometrical rules for cell division and a low time-correlation parameter γ. The second phase (stress-dominated, high ρ) shows poor agreement to geometrical rules and high temporal correlations. The transition between the two is continuous, as seen in panel **(b)**, showing the transition at fixed stress fractional penetration length $\zeta = 1/6$ (γ in red triangles, right vertical scale; α in blue dots, left vertical scale). Black vertical bars give the standard deviations for 20 randomly simulated values of the ratio $\lambda_c/(\kappa_c L_0^3)$. Panel **(c)** shows the consequences of this transition on the global tissue shape: above the critical value ρ_c, the shape of the whole tissue start being affected by the externally-induced mechanical stimuli. This is a consequence of the time correlations of division orientations, building up in the tissue due to long-range mechanical cues. The dynamics of stress propagation can be clearly read in the shape of the clones (collection of all progeny) of each of the 20 initial cells. These predictions were tested in the development of the epidermis of embryos of *P. mammillata* (panel **(d)**) which, due to shape changes of invaginating cells during gastrulation, shows the same transition in clones shape and cellular distribution. Embryonic 3D reconstruction from [34], visualized in MorphoNet [7].

Thanks to the availability of several 3D reconstructions of live embryonic development [34], we analysed division orientations and apical geometry of epidermal cells in two embryos of *P. mammillata* (see Appendix B for details): the coexistence of these two phases is observed *in vivo*, and elongated epidermal clones are built up while following the active shape changes of gastrulation as exemplified in Fig. 4(d). The clones cellular distribution observed in this process is the same as the one predicted by Eq. (4). In addition, the overall tissue shape shows the same structure as the high-stress tissues of Fig. 4(e), with a similar phase transition marked by a change in α from 0.7 ± 0.01 to 0.6 ± 0.03 and in γ from 0.3 ± 0.03 to 0.51 ± 0.04.

IV. CONCLUSIONS

In this work, we suggest a mechanism by which developing biological structures maintain a global coherence in spite of local radical changes in their form. Thanks to a reformulation

of the process of cytokinesis in terms of its energetic cost, we have shown that, through oriented cell division, cells can read and react to shape dynamics of their local and far-away environments (both of which alter the local stress state perceived by cells) by minimizing the work spent against the passive resistance of their surroundings. The cell's main geometrical axis emerges as the direction along which the work performed during division by a cell against the passive resistance of its local environment is minimal. However active processes of shape dynamics can bias such energetic cost and provide multiscale cues to guide cell division, in agreement with what reported, for instance, in the *Arabidopsis* meristem [25]. In these cases, reproducible and systematic deviations from long-axis rules emerge, as repeatedly experimentally reported [25–27]. The competition between local and long-range stimuli gives rise to a transition between two distinct phases of a multicellular system, marked by the onset of time-correlations within cellular clones. Remarkably the co-existence of these two phases, predicted by our model, is found *in vivo* in the epidermis of the developing embryo of the ascidian *P. mammillata*.

Our theory is able at once to explain the known geometrical rules for cell division and the systematic deviations from them. Both geometrical rules and deviations emerge as particular cases of a more general rule, which is the consequences of an energy exchange between a dividing cell and its environment. This exchange provides a way by which cells can sense and react to external mechanical forces, even for intensities below the minimal value to induce a meaningful cell strain. In this way, tissue deformation and shape dynamics can be produced without the need of individual cell deformations. Our result sheds new light on the physics of morphogenesis and on the mutual interplay between morphodynamics and mitosis, and suggest that oriented cell division is one of the contributing mechanisms allowing long-range transfer of information in biological structures. Such information transfer, under the form of internal mechanical stress, can be read in the shape of cellular clones within a proliferating tissue, providing a new paradigm to infer and follow force dynamics in living systems.

ACKNOWLEDGMENTS

PL and EF were members of CNRS, CG were a member of INRIA. Work in PL and CG's teams was funded by the Dig-Em project (ANR-14-CE11-0013-01) and the Institut de Biologie Computationnelle of Montpellier (IBC; ANR-11-BINF-0002). JL was supported by Dig-Em, BL by Dig-Em and IMPULSION project Mecafield from IDEXLYON. The authors wish to thank Dr. L. Guignard and Dr. U.-M. Fiuza for their outstanding efforts in making 3D reconstructions of ascidian embryos available; and Dr. O. Hamant and Dr. O. Ali for carefully reading the manuscript and for fruitful discussions.

All authors contributed to the conception of the original idea. BL developed the theory and the physical model, performed simulations, analysed datasets and results and wrote the paper; JL and EF contributed to the development of the theory and its connection to ascidian embryos; JL prepared datasets for analysis; PL and CG contributed to the development of the theory and the interpretation of results. All authors contributed to the writing of the paper and to the discussion and interpretation of the main results.

Appendix A: Random simulations of isolated cells

To test the agreement between Eq. (2) and either Hertwig's rule or the cell junctions rule, we have simulated divisions for 10^4 cells, whose geometry and vertex distribution was randomly chosen as follows:

- each cell was given as a collection of vertices lying along the perimeter of an ellipse;
- for each cell, the vertex number was a random integer drawn from the interval $[4, 50]$ with uniform probability;
- randomly drawn vertices were selected to be positioned at irregular angles, while the rest were placed along the ellipse's perimeter at the expected positions of a regular angular distribution;

- the angular position of each irregular vertex with respect to the ellipse center was drawn at random from a Gaussian distribution, centred on the angular position of a regular vertex and with constant standard deviation $\sigma_v = 0.3\,\mathrm{rad}$;

- the eccentricity of each ellipse was randomly drawn out of a uniform distribution over the interval $[0.2, 1)$ in order to avoid shapes without clear geometrical cues;

- the in-plane orientation of each ellipse's major axis, which gives also the cell's long axis, was randomly simulated by drawing two numbers x_v and y_v out of a gaussian distribution of zero mean and unit variance and using then the vector $\mathbf{n}_a = \frac{1}{|(x_v,y_v)|}(x_v, y_v)$;

- the main direction of cellular junctions was calculated by a principal-component analysis of each cell's vertices distribution in plane.

Appendix B: *P. mammillata* embryonic epidermal cells and analysis of their division directions

In order to calculate main elongations and division directions of cells in the embryonic epidermis of *P. mammillata*, we started from the cell-level 3D volume reconstruction of two whole embryos produced in [34].

On these embryos, thanks to their invariant lineage, cells over several generations can be unambiguously named [39, 40]. At the 64-cell stage, symmetric pairs of cells a7.11, a7.12, a7.13, a7.14, a7.15, a7.16, b7.11, b7.12, b7.13, b7.14, b7.15 and b7.16 were selected, corresponding to cells who will give rise to the embryonic epidermis after fate determination (green cells in Fig. B.1).

Each of these cells and their epithelial progeny for up to three rounds of division have been selected along the timestack of 3D volume reconstruction of each of the five chosen embryos. It being known that division of these cells always happens within the local tangential plane given by each cell's apical surface, to determine their main elongation we first selected their apical surfaces only out of the full 3D information on cell

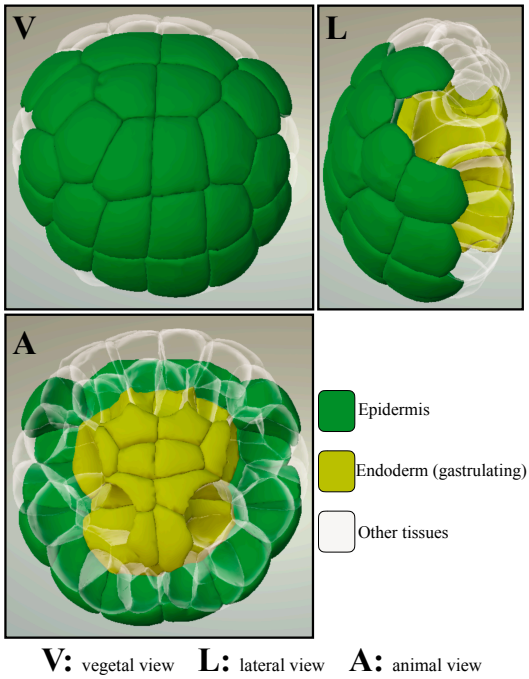

FIG. B.1: Reconstruction of a gastrulating embryo of *P. mammillata* [34]. Epidermal cells are labeled in green and endodermal cells (actively changing their shape) in yellow. Transparent cells belong to other embryonic tissues. Data visualized in MorphoNet [7].

shapes. For each cell i, we performed a principal component analysis on its apical surface to determine the direction of its main elongation $\hat{\mathbf{l}}^{(i)}_{\text{apical}}$ and the position of its center of mass $\mathbf{b}^{(i)}_{\mathbf{apical}}$. Finally, division direction of a cell i was defined as the direction $\hat{\mathbf{d}}^{(i)}_{\text{apical}}$ of the line joining the apical centers of mass $\mathbf{b}^{(i_1)}_{\mathbf{apical}}$ and $\mathbf{b}^{(i_2)}_{\mathbf{apical}}$ of its two daughter cells i_1, i_2. The directions $\hat{\mathbf{l}}^{(i)}_{\text{apical}}$ and $\hat{\mathbf{d}}^{(i)}_{\text{apical}}$ are sufficient to calculate the parameters $\Delta_{\text{HR}}, \alpha$ and γ shown in Figures 3,4.

[1] M. Dicko, P. Saramito, G. B. Blanchard, C. M. Lye, B, Sanson, and J. Étienne, *Geometry can provide long-range mechanical guidance for embryogenesis*, PLOS Comput. Biol. **13**, e100544 (2017).

[2] E. Paluch and C.-P. Heisenberg, *Biology and Physics of Cell Shape Changes in Development*, Curr. Biol. **19**, R790 (2009)

[3] J. Delile, M, Herrmann, N, Peyriéras, and R. Doursat, *A cell-based computational model of early embryogenesis coupling mechanical behaviour and gene regulation*, Nature Comm. **8**, 13929 (2016).

[4] A. R. Kherlopian *et al.*, *A review of imaging techniques for systems biology*, Bmc. Syst. Biol. **2**, 74 (2008).

[5] P. J. Keller, *Imaging morphogenesis: technological advances and biological insights*, Science **340**, 1234168 (2013).

[6] K. McDole, L. Guignard, *et al.*, *In Toto Imaging and Reconstruction of Post-Implantation Mouse Development at the Single-Cell Level*, Cell **175**, 859 (2018).

[7] B. Leggio, J. Laussu, A. Carlier, C. Godin, P. Lemaire, and E. Faure, *MorphoNet: an interactive online morphological browser to explore complex multi-scale data*, Nature Comm. **10**, 2812 (2019).

[8] D. W. Thompson, *On Growth and Form* (Dover, New York, 1942).

[9] U. S. Schwarz and S. A. Safran, *Physics of adherent cells*, Rev. Mod. Phys. **85**, 1327 (2013).

[10] C.-P. Heisenberg and Y. Bellaïche, *Forces in Tissue Morphogenesis and Patterning*, Cell **948**, 153 (2013).

[11] M. Uroz *et al.*, *Regulation of cell cycle progression by cell-cell and cell-matrix forces*, Nature Cell Biology **20**, 646 (2018).

[12] S. Nam and O. Chaudhuri, *Mitotic cells generate protrusive extracellular forces to divide in three-dimensional microenvironments*, Nature Physics **14**, 621 (2018).

[13] B. I. Shraiman, *Mechanical feedback as a possible regulator of tissue growth*, Proc. Natl. Acad. Sci. **102**, 3318 (2005).

[14] O. Hamant *et al.*, *Developmental Patterning by Mechanical Signals in Arabidopsis*, Science **322**, 1650 (2008).

[15] O. Wartlick, P. Mumcu, F. Jülicher, and M. Gonzalez-Gaitan *Understanding morphogenetic growth control - lessons from flies*, Nature Reviews Molecular Cell Biology **12**, 594 (2011).

[16] H. Oliveri, J. Traas, C. Godin, and O. Ali, *Regulation of plant cell wall stiffness by mechanical stress: a mesoscale physical model*, J. Math. Biol. **78**, 625 (2019).

[17] O. Hertwig, *Das Problem der Befruchtung und der Isotropie des Eies. Eine Theorie der Vererbung*, Jenaische Zeitschrift fur Naturwissenschaft **18**, 274 (1884).

[18] T. E. Gillies and C. Cabernard, *Cell Division Orientation in Animals*, Curr. Biol. **21**, R599 (2011).

[19] F. Bosveld *et al.*, *Epithelial tricellular junctions act as interphase cell shape sensors to orient mitosis*, Nature **530**, 495 (2016).

[20] L. Errera, *Sur une condition fondamentale d'équilibre des cellules vivantes*, C. R. Hebd. Seances Acad. Sci. **103**, 822 (1886).

[21] S. Besson and J. Dumais, *Universal rule for the symmetric division of plant cells*, Proc. Natl. Acad. Sci. **108**, 6294 (2011).

[22] A. Pierre, J. Sallé, M. Wühr, and N. Minc, *Generic Theoretical Models to Predict Division Patterns of Cleaving Embryos*, Dev. Cell **39**, 667 (2016).

[23] T. P. J. Wyatt *et al.*, *Emergence of homeostatic epithelial packing and stress dissipation through divisions oriented along the long cell axis*, Proc. Natl. Acad. Sci. **112**, 5726 (2015).

[24] W. T. Gibson *et al.*, *Control of the Mitotic Cleavage Plane by Local Epithelial Topology*, Cell **144**, 42 (2011).

[25] M. Louveaux, J.-D. Julien, V. Mirabet, A. Boudaoud, and O. Hamant, *Cell division plane orientation based on tensile stress in Arabidopsis thaliana*, Proc. Natl. Acad. Sci. **113**, E4294 (2016).

[26] E. Scarpa, C. Finet, G. B. Blanchard, and B. Sanson, *Actomyosin-Driven Tension at Compartmental Boundaries Orients Cell Division Independently of Cell Geometry In Vivo*, Dev. Cell **47**, 727 (2018).

[27] T. M. Finegan *et al.*, *Tissue tension and not interphase cell shape determines cell division orientation in the Drosophila follicular epithelium*, The EMBO Journal **38**, e100072 (2019).

[28] C. Cadart *et al.*, *Exploring the Function of Cell Shape and Size during Mitosis*, Dev. Cell **29**, 159 (2014).

[29] N. Ramkumar and B. Baum, *Coupling changes in cell shape to chromosome segregation*, Nat. Rev. Mol. Cell Biol. **17**, 511 (2016).

[30] J.W. Sanger and J.M. Sanger, *Surface and Shape Changes During Cell Division*, Cell Tissue Res. **209**, 177 (1980).

[31] S. Le Bras and R. Le Borgne, *Epithelial cell division - multiplying without losing touch*, J. Cell Sci. **127**, 5127 (2014).

[32] T. Lecuit and P.-F. Lenne, *Cell surface mechanics and the control of cell shape, tissue patterns and morphogenesis*, Nat. Rev. Mol. Cell Biol. **8**, 633 (2007).

[33] S, Alt, P. Ganguly, and G. Salbreux, *Vertex models: from cell mechanics to tissue morphogenesis*, Phil. Trans. R. Soc. B **372**, 20150520 (2017).

[34] L. Guignard, U.-M. Fiuza, *et al.*, *Contact-dependent cell-cell communications drive morphological invariance during ascidian embryogenesis*, bioRxiv: https://doi.org/10.1101/238741 (2017).

[35] G. Forgacs and S. A. Newman, *Biological Physics of the Developing Embryo* (Cambridge University Press, 2005).

[36] P. Lemaire, *Evolutionary crossroads in developmental biology: the tunicates*, Development **138**, 2143 (2011).

[37] K. Sherrard, F. Robin, P. Lemaire, and E. Munro, *Sequential Activation of Apical and Basolateral Contractility Drives Ascidian Endoderm Invagination*, Curr. Biol. **20**, 1499 (2010).

[38] G. Charras and A. S. Yap, *Tensile Forces and Mechanotransduction at Cell–Cell Junctions*, Curr. Biol. **28**, R445 (2018).

[39] E. G. Conklin, *The organization and cell - lineage of the ascidian egg* (Philadelphia :[Academy of Natural Sciences], 1905).

[40] M. Brozovic *et al.*, *ANISEED 2017: extending the integrated ascidian database to the exploration and evolutionary comparison of genome-scale datasets.*, Nucleic Acids Res. **46**, D718 (2018).